SIMULATION OF PREMIXED AND PARTIALLY PREMIXED JET-IN-CROSSFLOW FLAMES AT HIGH-PRESSURE

Bernhard Stiehl
University of Central Florida
4000 Central Florida Blvd, Orlando, FL 32816
bernhard.stiehl@knights.ucf.edu

Michelle Otero
University of Central Florida
4000 Central Florida Blvd, Orlando, FL 32816
michelleotero@knights.ucf.edu

Tommy Genova
University of Central Florida
4000 Central Florida Blvd, Orlando, FL 32816
tommy.genova@knights.ucf.edu

Tyler Worbington
University of Central Florida
4000 Central Florida Blvd, Orlando, FL 32816
tworbington@gmail.com

Jonathan Reyes
University of Central Florida
4000 Central Florida Blvd, Orlando, FL 32816
jonathan.reyes@ucf.edu

Scott Martin
Embry-Riddle Aeronautical University
600 S Clyde Morris Blvd, Daytona Beach, FL 32114
martis38@erau.edu

Carlos Velez
General Electric Company
1 Research Cir, Niskayuna, NY 12309
velezcar@yahoo.com

Kareem Ahmed
University of Central Florida
4000 Central Florida Blvd, Orlando, FL 32816
kareem.ahmed@ucf.edu

ABSTRACT

In this paper we explore the operational map of a lean axial-staged combustor of premixed and partially premixed reacting jet-in-crossflow flames at high-pressure (5 atm). This study attempts to expand the data to relatively high pressure and could significantly aid scaling to real gas turbine engine conditions at 20-30 atm. High speed camera, PIV, CH chemiluminescence, temperature and pressure measurements were taken and processed to allow accurate reconstruction of six operating points relative to CFD simulations under minimal adjustments. Variation of lean main stage (φ = 0.575 and 0.73) and rich jet (φ = 1.1, 4 and 8) equivalence ratio has been investigated for a four mm axial jet. The fully premixed flames were found to be controlled by the crossflow temperature before ignition and the crossflow oxygen content during combustion. Analysis of flame shape and position for the partially premixed operating points describes a lee stabilized as well as a more unsteady windward flame branch. Adjustment of added jet fuel and crossflow temperature along with its corresponding oxygen level is required to attain a compact flame body. The risk of delaying combustion progress is significantly increased at a richer jet φ = 8 and an overshooting, spatially divided flame was attained with a main stage φ = 0.73. Control towards a compact flame body is critical to allow combustion at reasonable reaction rate.*

Keywords: Axial Staged Combustion, Reacting Jet in Crossflow, Axial Fuel Staging, Gas Turbine Combustor, High Pressure

1. INTRODUCTION

Jet-in-crossflow is a canonical flow field that has been intensively studied for industrial application for several decades. Apart from its occurrence in exhaust plumes of power plants and its use for thrust vector control of high speed air-breathing systems and rocket vehicles [1], the main application is in the field of axial-staged gas turbine combustors for its potential to reduce NO_x emissions [2-5]. OEM patents were termed *Late Lean Injection* by GE [6, 7] and *Secondary Fuel Injection* by Siemens [8, 9]. Previous research in this field has significantly enhanced knowledge about short-chain fuel flames and ignition [10-15], pressure [16], influence of premixing [17, 18], formation of NO_x [19] and detailed flow characteristics [20, 21].

Closely related investigations about flame behavior determined for a premixed ethylene/air jet in their lean axial-staged combustor have been made by [22-24]. An unsteady windward branch stabilized by auto-ignition was observed along with a steadily attached leeward flame, stabilized by premixed flame propagation [24]. Additional details about those windward flame stabilization behaviors, which were named complete flame attachment, unsteady lifted flame, and windward blow-off, were supplied in [22]. All average windward flames were lifted, and liftoff heights strongly correlated to the momentum flux ratio. Blending with hydrogen might aid flame stability [25].

Indication of flame stabilization mechanisms has been observed for the partially premixed flames of this study, showing the windward ignition point move in a stream-wise domain of ±1.5d. Scope of the present paper has thereof been defined in verifying the findings of [22-24] for the fuel methane as well as extending the study to partially premixed flames.

2. RESEARCH OBJECTIVE

Fuel-only flames were shown to extend far downstream [26] and would overshoot into an attached turbine section, which is not desirable for industry application. We have thus extended our lean axial-staged combustor area of application towards premixed and partially premixed operating points. This paper studies variation of jet equivalence ratio (φ_{axial} = 1.1, 4, 8) with its corresponding parameter methane mass ($\dot{m}_{axial}^{CH4}$ = 0.957 g/s, 3.48 g/s, 6.96 g/s) to account for various fuel splits as well as variation of headend equivalence ratio (φ_{main} = 0.73, 0.575) with its corresponding parameters maximum temperature (T_{main}^{max} = 1918 K, 1623 K) and main stage oxygen mass fraction (w_{main}^{O2} = 0.060, 0.096) to account for various gas turbine loads. Data of these six experimentally verified axial-staged combustor operating points were processed and used for description by a single 3D CFD approach with minimal adjustment of models (flame propagation) and boundary conditions (temperature and headend species composition) to ensure comparability of the simulation.

3. EXPERIMENT AND DIAGNOSTICS

3.1 Experimental facility

The experimental facility is displayed in fig. 1. It contains a headend burner which provides vitiated crossflow to the axial stage with quasi-uniform boundary conditions.

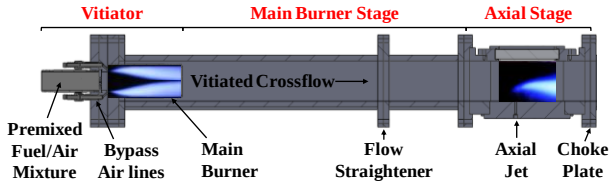

Figure 1: Experimental axial-staged combustor test facility

Methane and air react in the main burner pipe at lean conditions, and bypass air is injected coaxially around the main burner pipe to further lean out the vitiated flow. The axial stage consists of an optically accessible test section with two (124x95.2) mm side windows, a (127x40.6) mm bottom window, and a top injector plate with a 4 mm wall flush injector. At the exhaust of the facility is a choke plate with a 38.0 mm choke diameter to pressurize the flow to five atmospheres [26].

3.2 Flow control equipment

The main, bypass, and axial air were all metered using restriction orifice unions from *Global Industries* while the fuel flow rates were metered using *O'keefe* precision orifices. Pressure measurements were made by *Dwyer* pressure transmitters and recorded through *Labview* to determine mass flow rates. The headend of the facility is tuned to produce temperatures and NO_x levels similar to that of a real-world power generating gas turbine. Centerline temperature measurements were made using an exposed bead b-type thermocouple.

3.3 Experimental data processing

High speed line of sight CH* chemiluminescence data at 200 microns per pixel spatial resolution was taken using a *Photron Fastcam SA1.1* at a rate of 10,000 fps; a 430 nm filter was utilized to obtain CH* intensity. The images were processed in *Matlab* and time-averaged images were obtained considering 4000 images per data set. Flame boundaries were determined based on a CH* intensity gradient threshold set visually by observing where the flame lights off. This experimental CH* iso-level at certain I/I_{max} was

compared to the similar iso-level of the normalized progress variable from the CFD. Figure 2 shows the lee-side overlay of both signals for a φ_{axial} = 8 flame.

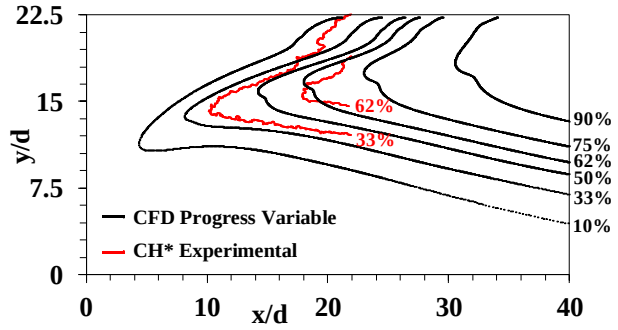

Figure 2: Comparison of experimental and CFD reaction progress normalized iso-levels at a φ_{axial} = 8

Particle image velocimetry (PIV) was performed using a dual 532 nm *Evergreen* laser and an *Andor* camera with a delay time of 20 μs between laser pulses at 12.5 Hz. 3 μm aluminum oxide (Al_2O_3) particles were used to seed the flow and were tracked using *PIV Lab* to obtain velocity fields.

4. COMPUTATIONAL MODEL

This *Star-CCM+* CFD model was built up in close accordance to previous numerical investigations [27, 28], focused on the critical jet-in-crossflow section of the axial-staged combustor. The coordinate system origin is defined at the point of collision between the jet and crossflow, as shown in fig. 3. Symmetry along the *z* axis has been utilized.

4.1 Mesh grid

A single structured mesh grid was used with a *Prism Layer Thickness* of 0.4 mm and total count of 20 million cells. Figure 3 depicts the computational domain with its dimensions in [mm] and local mesh refinement zones describing the fuel line, mixing and

ignition domain (1) at a grid size Δs = 0.125 mm as well as the *CVP* dissipation domain (2) at Δs = 0.25 mm. Grid convergence was shown and the highest residual levels were below 0.1% for the 20 million cell mesh grid.

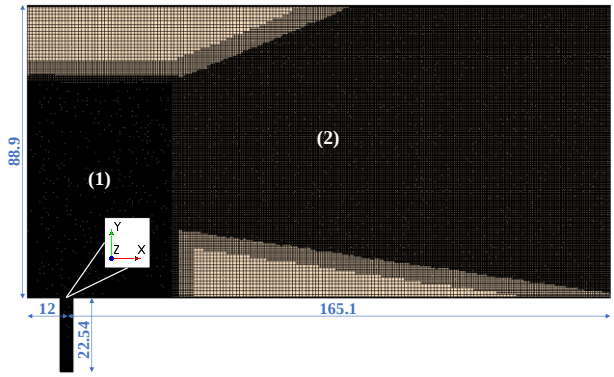

Figure 3: Axial Stage computational domain with dimensions in [mm] and mesh grid with local refinement zones

The simulations ran on a CentOS 7 cluster with Intel Xeon cores, x86_64 architecture with 32 cores and 128-192 GB RAM per node. Data was connected to a Lustre parallel file system with 56Gbit/s 4x FDR InfiniBand network fabric. Power demand was 5000 CPU hours per simulation.

4.2 Reactive flow modeling

Reactive flow was described by the *Flamelet Generated Manifold* (FGM) approach [29] at its defaults. Flamelet tables were generated in *Star-CCM+* from the *GRI Mech 3.0* [30], considering 15 species (CH_4, CH, CO, CO_2, H_2, H_2O, H_2O_2, HO_2, H, N_2, NO, NO_2, O_2, OH, O). To obtain a reasonable estimate of the crossflow oxygen level, the headend composition was defined at equilibrium for the corresponding temperature. Data for heat loss ratio, progress variable, mixture fraction and their variances were tabulated using the *1D Premixed Reactor* and adaptive gridding method. Species weights of CO, CO_2, H_2 and

H_2O ran through the *Star-CCM+* optimizer from defaults for a similar composition [31]. *Turbulent Flame Closure* (TFC) was applied at flame propagation rate of 1.5 to match the experimental data of partially premixed flames (φ_{axial} = 4 and φ_{axial} = 8). Figure 4 depicts a side-view camera image of the test facility (α) with windward and leeward ignition points highlighted by green circles as well as the adjacent CFD result at a φ_{main} = 0.73, showing iso-levels between 10% and 99% of the normalized progress variable.

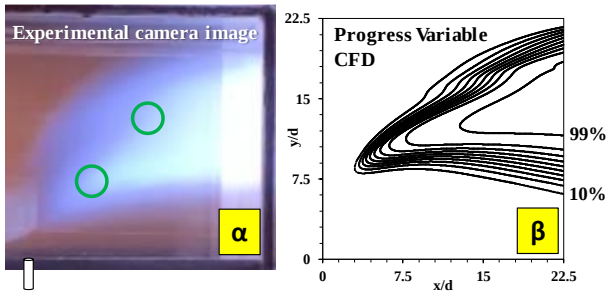

Figure 4: Experimental camera image (α) and CFD progress variable iso-levels (β) at a φ_{main} = 0.73

The premixed flames (φ_{axial} = 1.1) were modeled using the *Coherent Flame Model* (CFM) at a flame surface production coefficient increased from 1.5 to a value 2.0. All flames were locally ignited in the CFD with the corresponding pulsed progress variable (TFC) or flame area density (CFM) ignitor.

4.3 Headend flow profile and turbulence

Early imaging analysis pointed out the importance of stabilizing the headend flow to avoid acoustic instabilities and obtain a consistent boundary condition upstream of the jet-in-crossflow stage. The facility has been extended for an additional 152 mm section between the stages to a total reacting length of 1 m. Stabilized headend flow was experimentally confirmed with the PIV and the 3D field approximated by a sixth order

radial fit function (fig. 5) for the boundary condition in *Star-CCM+*. The result is a precise overlay of experimental and CFD data, confirming the measured headend centerline properties for $\varphi_{main} = 0.73$ ($T = 1918$ K, $v = 84.4$ m/s) as well as for $\varphi_{main} = 0.575$ ($T = 1623$ K, $v = 74.1$ m/s). Input velocities in the near-wall domain seem to deviate from the PIV data in fig. 5, but modelled results showed they were adequately accounted for by specification of no-slip wall condition and constant wall temperature of 400 K.

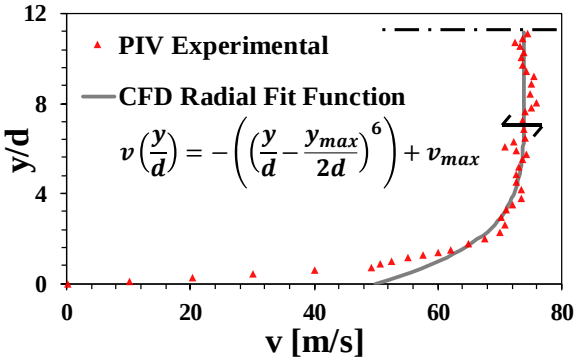

Figure 5: Experimental PIV data and radial 6th order CFD approximation at a $\varphi_{main} = 0.575$

The axial jet fuel line was modelled at adiabatic boundary condition. Influence of the boundary layer domain along the fuel line was numerically proven to increase penetration depth and could cover up to 75% of the cross-sectional area at fully developed flow condition and investigated Mach numbers between 0.6 and 0.8 for this 4 mm jet. To account for experimental non-idealities along the fuel line and at the hose fitting, inlet duct length was adjusted to result in a 40% boundary layer cross section at the point of contact with crossflow. Coupled flow model was used to account for compressible flow phenomena caused by these operating points at high subsonic Mach number. Turbulence was modeled as a steady *RANS* field according to [32] and parameter calibration was investigated [33]. Specified turbulence intensity levels are 12% at the crossflow inlet as determined from the

PIV and 5% at the jet inlet. Corrective action to match the experimental data was taken by adjusting the turbulent Schmidt and Prandtl numbers to 0.9, which is in the range defined by [34] for elevated momentum flux ratios (50-111). Further material properties were computed directly from the Flamelet table.

5. RESULTS AND DISCUSSION

5.1 Test matrix

Both the CFD and experimental investigations covered two headend equivalence ratios (φ_{main}) along with three equivalence ratios in the fuel line of the axial stage (φ_{axial}). Test conditions and numerical results are summarized in table 1. The temperature rise throughout the axial stage ΔT was determined by evaluating mass-weighted surface average function for cold and reacting flow at the outlet position, 40 jet diameters downstream of the jet. The momentum flux ratio J is defined in eq. 1:

$$J = \frac{\rho_{axial} * v_{axial}^2}{\rho_{main} * v_{main}^2} \tag{1}$$

Table 1 shows that the momentum flux ratios of the richest $\varphi_{axial} = 8$ case are higher compared to the cases with lower axial equivalence ratios due to the excess of axial fuel. Raising the main stage equivalence ratio from a $\varphi_{main} = 0.575$ to 0.73 was shown to increase the maximum headend temperature from 1623 K to 1918 K. For a φ_{main} of 0.73, addition of a certain axial fuel amount results in a smaller axial ΔT due to the higher amount of thermodynamic irreversibility at elevated temperature level. As table 1 further suggests, increasing the equivalence ratio of the axial stage would generally increase the total amount of axial heat release. However, the axial stage has a finite length, which is not sufficient to

allow complete combustion of non-premixed [27, 28] as well as low-level partially premixed flames. Therefore, heat release of the $\varphi_{main} = 0.575$, $\varphi_{axial} = 8$ flame did not reach its maximum value throughout the available axial stage geometry.

Table 1: Test Matrix for premixed and partially premixed operating points with a 4 mm axial jet at $p = 5$ atm

Headend					**Axial Stage**				
$\dot{m}_{main}^{CH4}$ **[g/s]**	$\dot{m}_{main}^{air}$ **[g/s]**	φ_{main} **[-]**	T_{main}^{max} **[K]**	w_{main}^{O2} **[-]**	$\dot{m}_{axial}^{CH4}$ **[g/s]**	$\dot{m}_{axial}^{air}$ **[g/s]**	φ_{axial} **[-]**	ΔT_{CFD} **[K]**	J_{CFD} **[-]**
20.3	486	0.73	1918	0.060	0.957	15.0	1.1	59	52.1
					3.48		4	186	80.5
					6.96		8	359	111
17.2	516	0.575	1623	0.096	0.957	15.0	1.1	61	50.7
					3.48		4	239	68.7
					6.96		8	320	95.7

5.2 Reacting jet penetration

Reacting jet penetration was investigated experimentally (triangles), numerically (solid lines) and empirically with correlation from Lefebvre (circles) in fig. 6. Particle traces of the jet trajectory have been acquired from *Star-CCM+*. Experimental camera images were recorded at minimal ambient light pollution and provide a clear outline of the mean reacting jet trajectory. Experimental uncertainties depend on the downstream position and could be up to 6%, mainly due to combustion instabilities along the windward flame branch. The experimental trends are accurately followed by the simulation, showing maximum deviations of 2.5% from the data.

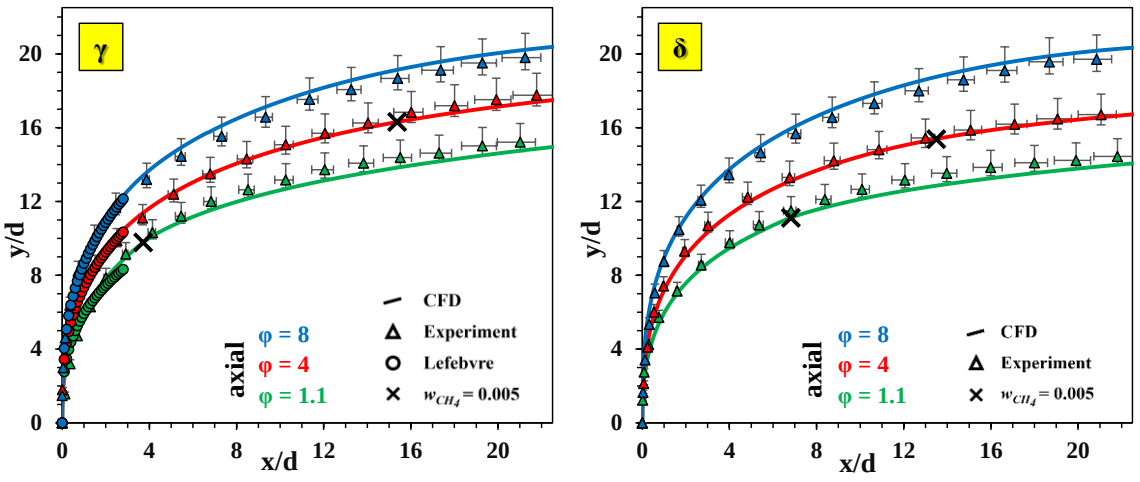

Figure 6: Reacting jet trajectories for d_J = 4 mm, p = 5 atm, φ_{main} = 0.73 (γ) and 0.575 (δ), J = 50.7–111

Correlation from Lefebvre [35] is defined in eq. 2

$$\frac{y}{d_{axial}} = 0.82 * J^{0.5} * \left(\frac{x}{d_{axial}}\right)^{0.33} \quad (2)$$

and has been overlaid for its valid definition range up to y_{max} (eq. 3), occurring after 2.8d downstream.

$$y_{max} = 1.15 * d_{axial} * J^{0.5} \quad (3)$$

The correlation is defined for non-reacting jets-in-crossflow, it describes the φ_{axial} = 8 and φ_{axial} = 4 graphs well but would underestimate the φ_{axial} = 1.1 data due to proximity of the reactive domain. As shown from the CFD, a good indication of windward flame ignition is the point of w^{CH4} = 0.005, highlighted with a black cross in fig. 6. Due to the low amount of methane entering the crossflow at fully premixed state, the φ_{axial} = 1.1 cases are primarily controlled by the crossflow temperature and were shown to ignite earlier than cases at richer jet equivalence ratio. For the latter, data along the reacting jet trajectory could only capture the point of windward flame ignition. At a φ_{axial} = 4, the opposite trend

was found, showing the windward branch with a φ_{main} = 0.575 to ignite first, which is due to the higher crossflow oxygen level. For the cases at a φ_{axial} = 8, the windward branches did not ignite at all by the end of the viewing window. Further investigation of ignition kinetics and strength at the windward as well as the leeward flame branch has been conducted throughout the entire CFD domain (section 5.3).

5.3 Windward and leeward flame ignition

CFD data (gray, blue) were extracted using linearly spaced symmetry plane iso-levels with minimum CH mass fraction of 1E-8. Experimental CH* data (red) were processed to verify the flame shape by defining and extracting threshold intensities of the maximum chemiluminescent intensity I_{max}.

5.3.1 Axial jet equivalence ratio of 1.1

Analysis of two premixed flames at φ_{axial} = 1.1 is shown as (A) and (B) in fig. 7.

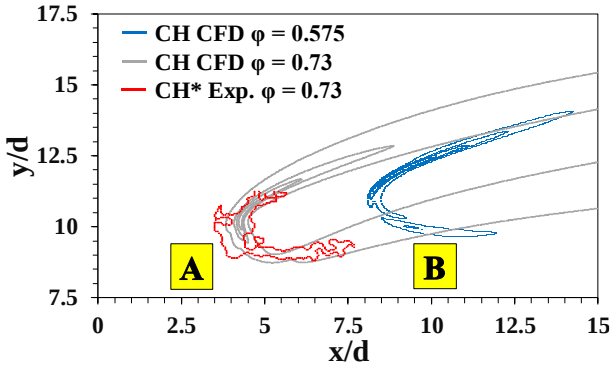

Figure 7: CH of premixed CH_4 flames at a φ_{axial} = 1.1, d_J = 4 mm, p = 5 atm, (A) φ_{main} = 0.73, J = 52.1, (B) φ_{main} = 0.575, J = 50.7

Position of the φ_{main} = 0.73 case has been verified by cropping the experimental CH* chemiluminescence image and filtering at levels 65% and 67% of I_{max}. Ignition of these lean flames is controlled by the crossflow temperature level. The φ_{main} = 0.73 flame (A)

was shown to ignite after an *x/d* = 4 and at a lift-off height of 9d. The φ_{main} = 0.575 (B) case needs more space to overcome the thermal delay and ignition was predicted after 8d downstream at a lift-off height of 10d. As indicated by comparison of the 1E-8 w^{CH} iso-levels, reaction progress after ignition is dependent on the available crossflow oxygen content, allowing flame (B) to combust at enhanced rate, once ignited.

5.3.2 Axial jet equivalence ratio of 4

Investigations of two partially premixed flames at a φ_{axial} = 4 are denoted with (C) and (D) in fig. 8.

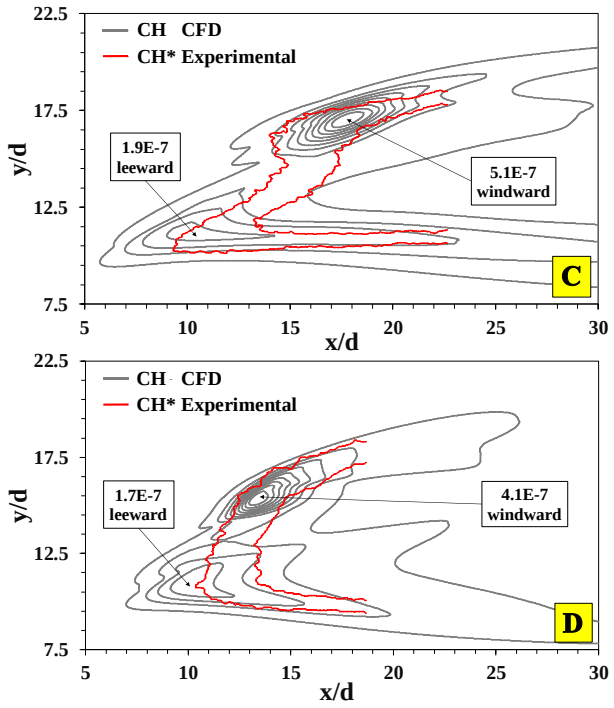

Figure 8: CH of partially premixed CH_4 flames at a φ_{axial} = 4, d_J = 4 mm, p = 5 atm, (C) φ_{main} = 0.73, J = 68.7, (D) φ_{main} = 0.575, J = 80.5

Maximum local CH mass fractions are indicated in the plots. The windward flame branch is located along the outer reacting jet trajectory (fig. 6) and characterized by elevated levels of lift in both x/d and y/d directions. The leeward flame branch is defined

as an early combustion event occurring at the inner lee-side of the jet trajectory and at lower y/d position.

For φ_{main} = 0.73 (C), experimental CH* data was extracted using the thresholds 84% and 99% of I_{max}. The CFD shows CH levels at downstream positions between *x/d* = 9 and *x/d* = 25 and an average lift-off height of 9d. It seems to be a slightly divided flame with dominant rich ignition point (w_{max}^{CH} = 5.1E-7) at the windward *Counter Rotating Vortex Pair* (*CVP*) branch after *x/d* = 18. The leeward side ignites early due to the high lean crossflow temperature and proximity of the windward ignition point.

Operating point with a more compact partially premixed flame has been attained by reducing the mainstage equivalence ratio. For the leaner φ_{main} = 0.575 (D), data at 65% and 92% of I_{max} were extracted. According to the CFD, the windward flame branch ignites 5d earlier than with flame (C) due to the increased crossflow oxygen content. CH levels are 10 – 20% lower than for flame (C), but local distribution of concentration is similar. Windward ignition dominates and induces an early leeward ignition after *x/d* = 10, but due to the lower crossflow temperature, this point is slightly further downstream than in flame (C). Concluding, the flame branches are better synchronized and allow formation of a more compact flame body. CH levels in (D) are slightly below levels in (C) but net reaction progress would still be greater due to the high w_{main}^{O2} level, allowing flame (D) to be combusted by *x/d* = 20.

5.3.3 Axial jet equivalence ratio of 8

Analysis of two partially premixed flames at a φ_{axial} = 8 are denoted with (E) and (F) in fig. 9. For the φ_{main} = 0.73 case (E), experimental data at 80% of I_{max} were extracted. High lean crossflow temperature aids an early leeward ignition with maximum CH levels

after x/d = 15, yet clearly the flame is limited by low oxygen levels at φ_{main} = 0.73, causing slow combustion progress throughout the axial stage. This visual observation was confirmed with the CFD, showing CH levels below w_{max}^{CH} = 1.6E-7 at both ignition points. The high jet fuel amount (φ_{axial} = 8) delays the rich windward ignition significantly to x/d = 40. Result is a flame that is torn apart, it may not be advisable to run at this condition. Length of the flame was shown in 3D to significantly overshoot the jet-in-crossflow stage along the *CVP*. Applied industrially, this flame would likely extend into an attached turbine section. Lift-off height is 11d.

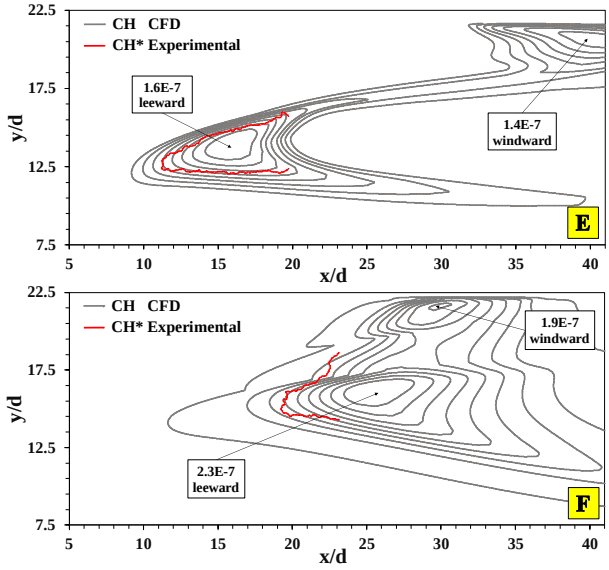

Figure 9: CH of partially premixed CH_4 flames at a φ_{axial} = 8, d_J = 4 mm, p = 5 atm, (E) φ_{main} = 0.73, J = 111, (F) φ_{main} = 0.575, J = 95.7

A reasonable flame shape was obtained for the leaner φ_{main} = 0.575 case (F). Experimental data were filtered at 62% of I_{max}. Windward and leeward flame are delayed due to the high fuel amount (ignition after 25d) and low temperature (ignition after 30d), respectively. Yet the rich windward branch ignited earlier than in (E) due to the increased oxygen level at φ_{main} = 0.575. The ignition points seem to interact and resulting CH levels

were determined to be w_{max}^{CH} = 1.9E-7 (windward) and 2.3E-7 (leeward), describing a 40% increase compared to flame (E). Transition zone between both flames was observed in the CFD and could be partially verified from the experimental image. Lift-off height is 13d and decreases due to diffusion, facilitated by its position being far downstream.

5.3.4 Observing mechanism

In a real combustor, any fixed lean headend temperature level would relate to a certain oxygen level at the headend, provided that further parameters are not varied. Two additional, partially premixed flames were simulated for definition of a valid prioritization of factors that influence windward and leeward ignition. Theoretical decrease of the O_2 level for the φ_{main} = 0.575 case with a φ_{axial} = 8 and unaltered remaining parameters resulted in barely any ignition of the windward branch throughout the domain. Leeward ignition was delayed for another 5 jet diameters. 3D analysis confirmed that barely any reaction rate could be pointed out at any position inside the *CVP*. In contrast, artificial increase of the crossflow O_2 level for the φ_{main} = 0.73 case resulted in a slightly earlier ignition of the windward branch (2.5d early at w_{main}^{O2}= 0.076), about 1d earlier ignition at the leeward side, and reaction rates in the *CVP* significantly increased for half an order of magnitude. These results confirm the trends observed from the data and allow formulation of an observing mechanism about parameters controlling the ignition of partially premixed, rich methane jets in a lean combustor.

a) Along the windward branch, ignition is accelerated primarily by reducing the jet mass flow $\dot{m}_{axial}^{CH4}$. Secondary factor promoting windward ignition is the increase of crossflow oxygen level w_{main}^{O2} and subordinate influence has the increase of crossflow temperature T_{main}.

b) At the leeward branch, ignition is facilitated by proximity of the windward ignition point, inducing an early leeward ignition. A secondary factor promoting ignition is the increase of T_{main}, but its weight is an order of magnitude lower. Subordinate influence on leeward ignition has an increased w_{main}^{O2}.

c) Throughout their investigated range of variation, role of crossflow oxygen levels is to shift both flame branches along the *x/d* axis.

Assessment of further parameters influencing partially premixed ignition could include variation of pressure level, preheating of the fuel line, or the use of different diluents.

6. CONCLUSION

The present investigations of premixed and partially premixed methane flames are targeted towards industry application in a lean axial-staged gas turbine combustor at a pressure of 5 atmospheres and with a 4 mm axial jet. Simplicity of the premixed flame body at a φ_{axial} = 1.1 helped isolate two major factors influencing the lean combustion regime. Firstly, low headend temperature was shown to result in an increased thermal delay before axial ignition, and secondly, high headend oxygen levels accelerated the axial reaction progress after ignition. For industry application, these premixed operating points would likely not be considered due to their low axial fuel amount and poor resulting fuel splits, assuming a reasonable mass flow of main stage fuel. Future investigations with the similar facility and a 12.7 mm axial jet will be required to generate a dataset of industrially relevant premixed flames.

Promising results were attained for the partially premixed flames. The investigations at a richer φ_{axial} = 4 resulted in stable flames with a compact flame body and high reaction rate, allowing the flame to close by the downstream end of the combustor. Plenty of margin for adjustment of headend temperature and crossflow oxygen level was proven to be available. Axial jet equivalence ratio φ_{axial} = 4 seems to provide the best starting point for fine-tuning towards industry application in a lean axial-staged gas turbine combustor with a 4 mm methane jet.

Industrial use of the rich φ_{axial} = 8, φ_{main} = 0.575 flame can be considered but fine-tuning of parameters would have to take place within a narrow value range, ensuring the flame remains at an undivided, compact shape. Role of crossflow oxygen level to shift both flame branches was determined. Main influence factor on the resulting flame shape is the proximity of both local ignition points, allowing synchronized, stabilized flames at lean crossflow equivalence ratio and burning at reasonable reaction rate. In contrast, a φ_{main} = 0.73 flame at φ_{axial} = 8 cannot be fine-tuned to fulfill industry needs, the flame is highly divided and would significantly overshoot any reasonably dimensioned jet-in-crossflow stage.

ACKNOWLEDGMENTS

The authors (BS, MO, TG, TW, JR, SM and KA) acknowledge support from the Department of Energy under Award Number DE-FE0031227 and collaboration with GE Global Research.

thereof, nor any of their employees, makes any warranty, express or implied, or assumes any legal liability or responsibility for the accuracy, completeness, or usefulness of any information, apparatus, product, or process disclosed, or represents that its use would not infringe privately owned rights. Reference herein to any specific commercial product, process, or service by trade name, trademark, manufacturer, or otherwise does not necessarily constitute or imply its endorsement, recommendation, or favoring by the United States Government or any agency thereof. The views and opinions of authors expressed herein do not necessarily state or reflect those of the United States Government or any agency thereof.

NOMENCLATURE

d	jet diameter, m
J	momentum flux ratio
$\dot{m}$	mass flow rate, kg/s
p	pressure, atm
s	cell dimension, m
T	temperature, K; °C
v	velocity, m/s
w	mass fraction
x	axial coordinate, downstream position, m
y	perpendicular coordinate, penetration depth, m

z	lateral coordinate, m

Greek Letters

Δ	difference
φ	equivalence ratio

Subscripts and superscripts

axial	axial stage
CFD	Computational Fluid Dynamics
J	jet
main	main burner stage
max	maximum

Acronyms and abbreviations

CFD	Computational Fluid Dynamics
CFM	Coherent Flame Model
CPU	Central Processing Unit
CVP	Counter Rotating Vortex Pair
FGM	Flamelet Generated Manifold
fps	frames per second
OEM	Original Equipment Manufacturer

RAM	Random Access Memory
PIV	Particle Image Velocimetry
RANS	Reynolds Averaged Navier Stokes
TFC	Turbulent Flame Closure

REFERENCES

[1] Karagozian, A. R., 2003, "Background on and Applications of Jets in Crossflow," Manipulation and Control of Jets in Crossflow, pp. 3-13.

[2] Pandaa, P. P., Busari, O., Roac, M., Lucht, R. P., 2019, "Flame stabilization mechanism in reacting jets in swirling vitiated crossflow," Combustion and Flame, 207, pp. 302-313.

[3] Schulz, O., Piccoli, E., Felden, A., Staffelbach, G., Noiray, N., 2019, "Autoignition-cascade in the windward mixing layer of a premixed jet in hot vitiated crossflow," Combustion and Flame, 201, pp. 215-233.

[4] Bandarua, R. V., Turns, S. R., 2000, "Turbulent jet flames in a crossflow: effects of some jet, crossflow, and pilot-flame parameters on emissions," Combustion and Flame, 121(1-2), pp. 137-151.

[5] Karim, H., Natarajan, J., Narra, V., Cai, J., Rao, S., Kegley, J., Citeno, J., 2017, "Staged Combustion System for Improved Emissions Operability & Flexibility for 7HA Class Heavy Duty Gas Turbine Engine," Proceedings of ASME Turbo Expo 2017, 10.1115/GT2017-63998.

[6] Venkataraman, K. K., Terry, J. C., Velkur, C. B., Karim, H., 2014, "Late Lean Injection Fuel Staging Configurations," General Electric Company.

[7] Venkataraman, K. K., Washam, R. M., Karim, H., Terry, J. C., Davis, L. B., 2014, "Late Lean Injection System Configuration," General Electric Company.

[8] Martin, S. M., Cai, W., Harris, J., 2013, "Apparatus and Method for Controlling the Secondary Injection of Fuel," Siemens Energy, Inc.

[9] Laster, W. R., Martin, S. M., Bilbao, J. E. P., Hardes, J., Fox, T. A., 2018, "Dual Outlet Nozzle for a Secondary Fuel Stage of a Combustor of a Gas Turbine Engine," Siemens Energy, Inc.

[10] Schlegel, F., Ghoniem, A. F., 2014, "Simulation of a high Reynolds number reactive transverse jet and the formation of a triple flame," Combustion and Flame, 161(4), pp. 971-986.

[11] Yi, T., Halls, B. R., Jiang, N., Felver, J., Sirignano, M., Emerson, B. L., Lieuwen, T. C., Gord, J. R., Roy, S., 2019, "Autoignition-controlled flame initiation and flame stabilization in a reacting jet in crossflow," Proceedings of the Combustion Institute, 37(2), pp. 2109-2116.

[12] Lin, H.-C., Cheng, T-S., Chen, B-C., Ho, C-C., Chao, Y-C., 2009, "A comprehensive study of two interactive parallel premixed methane flames on lean combustion," Proceedings of the Combustion Institute, 32(1), pp. 995-1002.

[13] Jaravel, T., Labahn, J., Sforzo, B., Seitzman, J., Ihme M., 2019, "Numerical study of the ignition behavior of a post-discharge kernel in a turbulent stratified crossflow," Proceedings of the Combustion Institute, 37(4), pp. 5065-5072.

[14] Steinberg, A. M., Sadanandan, R., Dem, C., Kutne, P., Meier, W., 2013, "Structure and stabilization of hydrogen jet flames in cross-flows," Proceedings of the Combustion Institute, 34(1), pp. 1499-1507.

[15] Sullivan, R., Wilde, B., Noble, D. R., Seitzman, J. M., Lieuwen, T. C., 2014, "Time-averaged characteristics of a reacting fuel jet in vitiated cross-flow," Combustion and Flame, 161(7), pp. 1792-1803.

[16] Schulz, O., Noiray, N., 2019, "Combustion regimes in sequential combustors: Flame propagation and autoignition at elevated temperature and pressure," Combustion and Flame, 205, pp. 253-268.

[17] Dayton, J. W., Linevitch, K., Cetegen, B. M., 2019, "Ignition and flame stabilization of a premixed reacting jet in vitiated crossflow," Proceedings of the Combustion Institute, 37(2), pp. 2417-2424.

[18] Marr, K. C., Clemens, N. T., Ezekoye, O. A. , 2012, "Mixing characteristics and emissions of strongly-forced non-premixed and partially-premixed jet flames in crossflow," Combustion and Flame, 159(2), pp. 707-721.

[19] Sirignano, M. D., Nair, V., Emerson, B., Seitzman, J., Lieuwen, T. C., 2019, "Nitrogen oxide emissions from rich premixed reacting jets in a vitiated crossflow," Proceedings of the Combustion Institute, 37(4), pp. 5393-5400.

[20] Nair, V., Wilde, B., Emerson, B., Lieuwen, T., 2019, "Shear Layer Dynamics in a Reacting Jet in Crossflow," Proceedings of the Combustion Institute, 37, pp. 5173-5180.

[21] Nair, V., Sirignano, M., Emerson, B., Halls, B., Jiang, N., Felver, J., Roy, S., Gord, J., Lieuwen, T., 2019, "Counter rotating vortex pair structure in a reacting jet in crossflow," Proceedings of the Combustion Institute, 37(2), pp. 1489-1496.

[22] Wagner, J. A., Grib, S. W., Renfro, M. W., Cetegen, B. M., 2015, "Flowfield measurements and flame stabilization of a premixed reacting jet in vitiated crossflow," Combustion and Flame, 162, pp. 3711–3727.

[23] Wagner, J. A., Renfro, M. W., Cetegen, B. M., 2017, "Premixed jet flame behavior in a hot vitiated crossflow of lean combustion products," Combustion and Flame, 176, pp. 521-533.

[24] Wagner, J. A., Grib, S. W., Dayton, J. W., Renfro, M. W., Cetegen, B. M., 2017, "Flame stabilization analysis of a premixed reacting jet in vitiated crossflow," Proceedings of the Combustion Institute, 36(3), pp. 3763-3771.

[25] Fleck, J. M., Griebel, P., Steinberg, A. M., Arndt, C. M., Naumann, C., Aigner, M., 2013, "Autoignition of hydrogen/nitrogen jets in vitiated air crossflows at different pressures," Proceedings of the Combustion Institute, 34(2), pp. 3185-3192.

[26] Genova, T., Otero, M., Stiehl, B., Reyes, J., Ahmed, K., Martin, S., 2019, "Exploration of a Reacting Jet-in-Crossflow in a High-Pressure Axial Stage Combustor," AIAA Propulsion and Energy 2019 Forum.

[27] Stiehl, B., Worbington, T., Woodard, A., Ahmed, K., 2020, "Numerical Simulation of an Axial-Staged Combustor at High Pressure," Scitech Session GTE-05, Combustors I.

[28] Stiehl, B., Worbington, T., Miegel, A., Martin, S., Velez, C., Ahmed, K., 2019, "Combustion and Emission Characteristics of a Lean Axial-Stage Combustor," Proceedings of ASME Turbo Expo 2019, 10.1115/GT2019-91796.

[29] Chan, W. L., Kolla, H., Chen, J. H., Ihme, M., 2014, "Assessment of model assumptions and budget terms of the unsteady flamelet equations for a turbulent reacting jet-in-cross-flow," Combustion and Flame, 161(10), pp. 2601-2613.

[30] Smith, G. P., Golden, D. M., Frenklach, M., Moriarty, N. W., Eiteneer, B., Goldenberg, M., Bowman, C. T., Hanson, R. K., Song, S., Gardiner, Jr., W. C. Lissianski, V. V. and Qin, Z., "GRI-MECH 3.0," http://www.me.berkeley.edu/gri_mech/.

[31] Ihme, M., Shunn, L., Zhang, J., 2012, "Regularization of reaction progress variable for applicationto flamelet-based combustion models," Journal of Computational Physics, 231, pp. 7715-7721.

[32] Karvinen, A., Ahlstedt, H., 2005, "Comparison of Turbulence Models in Case of Jet in Crossflow Using Commercial CFD Code," Engineering Turbulence Modelling and Experiments 6, pp. 399-408.

[33] Lefantzi, S., Ray, J., Arunajatesan, S., Dechant, L., 2013, "Tuning a RANS k-ε Model for Jet-in-Crossflow Simulations," Sandia Report SAND2013-8158.

[34] Tominagaa, Y., Stathopoulos, T., 2007, "Turbulent Schmidt numbers for CFD analysis with various types of flowfield," Atmospheric Environment, 41, pp. 8091-8099.

[35] Lefebvre, A. H., Ballal, D. R., 2010, Gas Turbine Combustion Alternative Fuels and Emissions Third Edition.

Table Captions List

Table 1: Test Matrix for premixed and partially premixed operating points with a 4 mm axial jet at p = 5 atm.....11

Figure Captions List

Figure 1: Experimental axial-staged combustor test facility 4

Figure 2: Comparison of experimental and CFD reaction progress normalized iso-levels at a φ_{axial} = 8..... 6

Figure 3: Axial Stage computational domain with dimensions in [mm] and mesh grid with local refinement zones 7

Figure 4: Experimental camera image (α) and CFD progress variable iso-levels (β) at a φ_{main} = 0.73..... 8

Figure 5: Experimental PIV data and radial 6th order CFD approximation at a φ_{main} = 0.575 9

Figure 6: Reacting jet trajectories for d_J = 4 mm, p = 5 atm, φ_{main} = 0.73 (γ) and 0.575 (δ), J = 50.7–111 12

Figure 7: CH of premixed CH_4 flames at a φ_{axial} = 1.1, d_J = 4 mm, p = 5 atm, (A) φ_{main} = 0.73, J = 52.1, (B) φ_{main} = 0.575, J = 50.7..... 13

Figure 8: CH of partially premixed CH_4 flames at a φ_{axial} = 4, d_J = 4 mm, p = 5 atm, (C) φ_{main} = 0.73, J = 68.7, (D) φ_{main} = 0.575, J = 80.5..... 14

Figure 9: CH of partially premixed CH_4 flames at a φ_{axial} = 8, d_J = 4 mm, p = 5 atm, (E) φ_{main} = 0.73, J = 111, (F) φ_{main} = 0.575, J = 95.7 16